Repair of damaged multiple leaf masonry: assessment by the Acoustic Emission technique

A. Anzani, L. Binda
Department of Structural Engineering, Politecnico di Milano, Italy

A. Carpinteri, G. Lacidogna and A. Manuello
Department of Structural Engineering and Geotechnics, Politecnico di Torino, Italy

ABSTRACT: Most historic centers in Italy are characterized by the presence of monumental buildings like churches and palaces, and also by a diffused built environment which itself constitutes an important part of the cultural heritage. The problem of safety of these historic masonry constructions started to attract increasing attention after the sudden collapse of ancient monuments happened in the last decades. In this work an experimental research has been carried out on three-leaf walls, using two stones of different characteristics trying to reproduce masonry typologies frequently used in Italian historic centres. Aim of the research was to understand the stress-strain behavior of this masonry under compression and shear actions and to find out suitable repair techniques. The application of the Acoustic Emission technique (AE), gave the possibility to interpret the damage mechanisms and to evaluate the effectiveness of the repair interventions, contributing to the determination of the most suitable methodology for their optimisation.

1 INTRODUCTION

Most historical centres in Italy are characterised not only by the presence of monumental buildings, but also by a man-made environment, which in itself constitutes an important part of the cultural heritage. Both monumental and minor architectural structures are often made of stonework masonry and were built using different techniques. In most cases they are made of the so-called multiple leaf stone masonry, the specific characteristics of which should be understood before undertaking a safety assessment on many kinds of structures. This is the case, for instance, when considering the seismic vulnerability of stonework buildings, but it also applies to the evaluation of the stability of ancient cathedrals, whose pillars have non-homogeneous cross-sections.

An experimental research was carried out on three-leaf walls built using two stones having different characteristics in an attempt to reproduce two masonry types frequently used in Italian historical city centres. The aim of the research was to understand the stress-strain behaviour of this masonry under shear actions and to investigate possible repair techniques. After shear testing, some specimens could be recovered and repaired by grout injections and steel rods confinement. The initial results obtained from the shear tests subsequently carried out on the repaired specimens to verify the effectiveness of the techniques adopted are discussed below.

For the localisation of damage, a sophisticated equipment for the analysis of AE signals was used. This equipment consists of six USAM® units for signal acquisition and processing. Each of these units analyses in real time, and transmits to a PC, all the characteristic parameters of an ultrasonic event. In this manner, each AE event is identified by a progressive number and characterized by a series of data giving the amplitude and the time duration of the signal and the number of oscillations. Each unit is equipped with a pre-amplified wide-band piezo-electric sensor (PZT), which is sensitive in a frequency range of 50 kHz to 800 kHz. The signal acquisition threshold can be set in a range of 100μV to 6.4 mV. As known, the cracking process inside the material subjected to compression and shear takes place through the formation of a quantity of micro-cracks. With increasing loads, these coalesce into macrocracks, whose formation brings about a reduction in the bearing capacity of the structures (Carpinteri & Lacidogna 2006, Carpinteri et al. 2007). The statistical techniques derived from seismology, such as the Gutenberg-Richter (GR) law, and the analysis performed in terms of Self Organized Criticality (SOC), mated to AE monitoring, clarify the relationships between microstructural events and the macroscopic behaviour of structures during the damaging process (Carpinteri 1994, Carpinteri et al. 2006, Richter 1958, Chen et al. 1991).

2 EXPERIMENTAL DETAILS

2.1 *Specimen preparation*

Three-leaf stone walls, measuring 310x510x790 mm^3, were built at DIS - Politecnico di Milano, by Spadaro srl Contractor - Rosolini, Sicily, so as to reproduce the morphology of the multiple-leaf walls and piers frequently encountered in historical centres (Fig. 1). The two external leaves, made of stone blocks with horizontal and vertical mortar joints, are connected to an internal rubble masonry leaf made of pebbles of the same kind of stone and connected with the same mortar as the outer leaves (Binda et al. 2003).
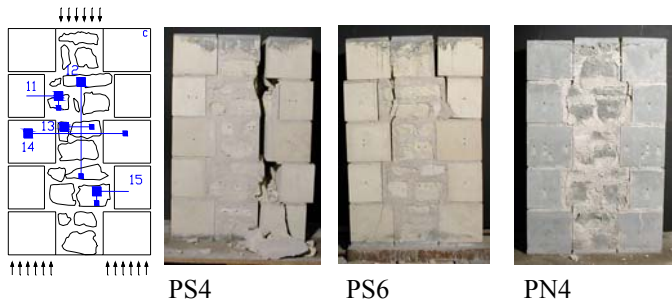

Figure 1. Loading condition and aspect of the specimens once removed from the testing machine.

Two types of stones were chosen: the same limestone used for the Noto Cathedral (Noto stone) and a sandstone, frequently used in central and southern Italy (Serena stone). The characteristics of the two stones were obtained on cylindrical specimens, 80mm in diameter and 160mm high, cored from regularly cut stones. Compressive strength (σ_c) was determined in both directions, normal and parallel to the bedding planes, and tensile strength (σ_t) was determined in the same direction as the bedding planes. The values of the elastic modulus (E_a) and Poisson's ratio (ν_a), determined as an average over 3 specimens, are given in Table 1.

Table 1. Characteristics of the stones

Stone σ_t	Load vs Bedding Planes Direction	σ_c	E_a	ν	
Noto	Normal	20,6	9476	0,10	2,06
Noto	Parallel	17,6	8526	0,09	-
Serena	Normal	104,2	18218	0,19	6,07
Serena	Parallel	89,0	23293	0,21	-

Compressive strength, elastic modulus and tensile strength are expressed in N/mm^2

2.2 *Pseudo-shear tests before and after repairs*

The walls were tested to failure in pseudo-shear conditions according to the loading scheme shown in Figure 1. Further details on the complete experimental campaign can be found in (Anzani et al. 2004, Binda et al. 2003).

Once removed from the testing machine and stored in the laboratory, the walls were repaired and subsequently tested again. The repair was carried out by means of grout injections designed to fill the main cracks formed at the interface between the inner and the outer leaves during the test and by fitting steel bars. In particular, completely inorganic mixes based on microfine pozzolanic binders were used (Modena et al. 2002) and rods, having a diameter of 16 mm and characterized by an elastic modulus of 19500 N/mm^2, were applied by tightening the nuts to a torque of 50 NM. This corresponds to a longitudinal action of 15.63 kN on each rod, corresponding in its turn to a total lateral confinement on each wall of 0.37N/mm^2.

2.3 *Analysis of the results*

The characteristic values reached through the shear tests before and after the repair and the techniques adopted to repair the specimens are given in Table 2. The results of the tests on the repaired specimens can be seen in Figure 2, 3 and 4, where the load vs. displacement diagrams are shown, compared to those obtained after the shear tests and before the repair.

Considering the different types of stone constituting the walls, the repair always caused an increase in load-bearing capacity, of 1.24 in the case of specimen PS4, made of Serena stone and repaired by grout injections only, more appreciable in the other cases.

Table 2. Characteristics of the walls tested before and after repair.

Wall	Repair	Virgin		Repaired	
		$P_{max,b}$ [kN]	δ_{max} [µm]	$P_{max,b}$ [kN]	δ_{max} [µm]
PS4	Injection	391,10	4056,84	485,33	2971,91
PS6	Steel Rods	415,89	4369,80	700,88	8462,52
PN4	Injection + Steel Rods	283,85	3631,31	520,17	6636,5

In the two cases where the repair was made through injections (PS4 and PN4), the subsequent collapse of the two collar joints, that could be clearly observed in the diagrams plotted before the repair, is no longer visible (Fig. 2). This is scarcely evident in the case of the wall repaired only with steel rods (PS6), in which case the diagram shows a small decrease, corresponding to a displacement of 6000 µm.

In the case of specimen PS6, the most ductile one because of the steel rods and the quality of the stone, the outer leaves did not crack. Failure took place through cracks propagation in the inner leaf, mostly involving the mortar at the interface with the stone pebbles, and at the interfaces between the inner and the outer leaves; cracks also propagated diagonally, indicating the diffusion of the load, and presented a concentration resulting in the detachment of material from the second stone layer below the top.

In the case of specimen PN4 a greater involvement of the outer leaf was observed at failure, when new cracks opened and, in some areas, delamination occurred, together with the propagation in the inner

leaf of cracks that sometimes also cut the stone pebbles. In this case horizontal cracks were also visible, both in the outer leaf and in the inner leaf at the base level, due to the compression effect produced horizontally by the presence of the steel rods during the loading phase, given the low strength of the stone.
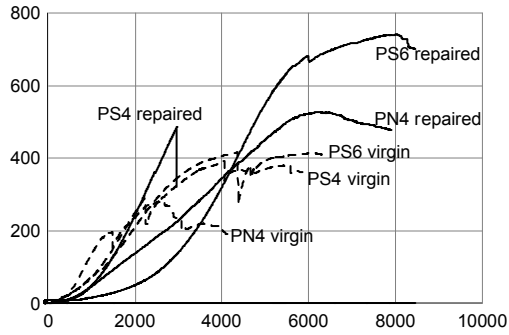

Figure 2. Results on virgin and repaired specimens.

Figures 3a - 5a show the shear stress vs. strain diagrams obtained from the readings of single LVDTs, whereas Figures 3b - 5b show the load vs. relative displacement diagrams from LVDTs placed at the interface between the inner and outer leaves. Conventionally, shortening was plotted as positive and elongation as negative; apart from some anomalous readings indicated below, vertical strains were always positive and horizontal ones were always negative.
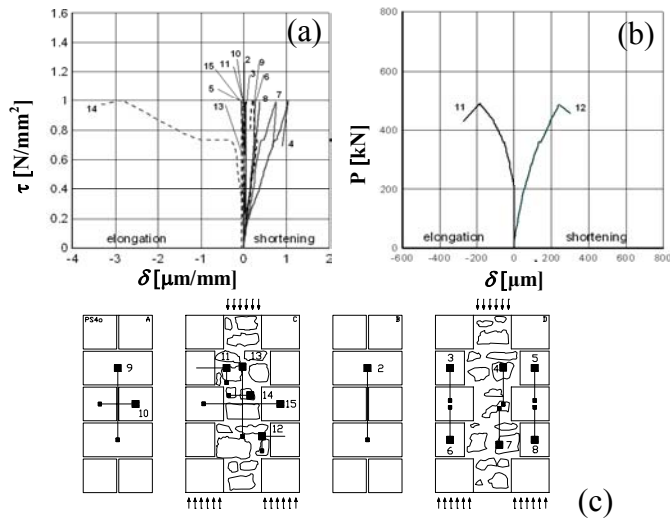

Figure 3. Results on specimen PS4.

In the case of wall PS6, repaired only with steel rods (Fig. 4b), the values recorded by both the LVDTs measuring the relative displacement were higher than in the other walls, consistently with the presence of previous cracks at the interface that had not been filled and in agreement with the compliant behaviour mentioned above. In the case of wall PN4 only LVDT 5, having a longer base, gave higher values than the other vertical LVDTs, which all showed very similar strains. This indicates that, in the case of Noto stone, which is characterised by a high porosity, a good adhesion developed, as borne out by the first series of test (Binda et al. 2003), during which similar strains were observed in the inner

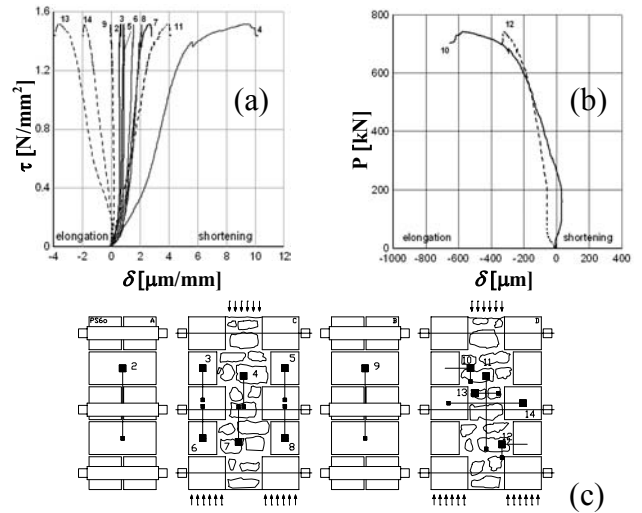and outer leaves, with essentially no relative displacements at the interface.

Figure 4. Results on specimen PS6.

This is also confirmed in Figure 3b by the virtually nil readings from LVDT 3 (placed in a high position). The readings from LVDT 4 do not indicate a relative displacement, mostly because, given the considerable length of the transducer base, they are influenced by the shortening effect of the inner leaf. Moreover, the presence of the steel rods probably played a role in reducing the displacements, given the contribution of frictions.
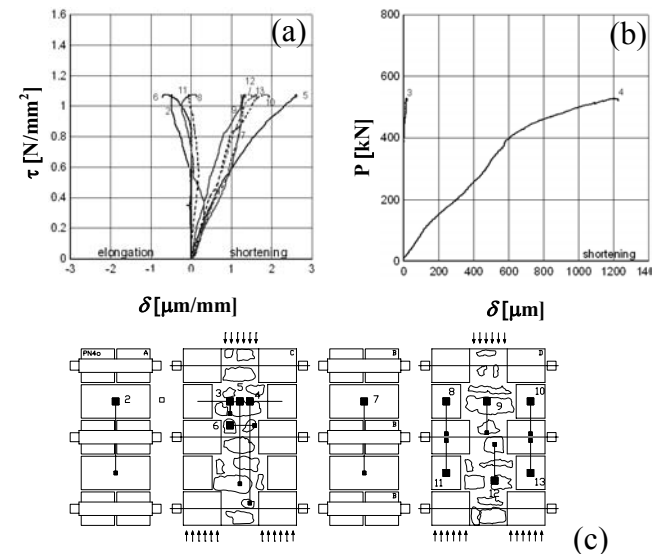

Figure 5. Results on specimen PN4.

3 AE MONITORING

Acoustic emissions are ultrasonic waves; generated by a rapid release of energy, coming from discontinuities or cracks propagating in materials subject to states of stress or strain. In isotropic and homogeneous materials, the waves propagate through the damaged solid, according to straight paths, moving at the same rate v in every direction, until they reach the outer surface, where they are captured by ad hoc sensors (Carpinteri & Lacidogna 2006, Carpinteri et al. 2007). The process is similar to the one that takes

place in seismology, where the elastic waves generated by the earthquakes reach the monitoring stations positioned on the surface of the earth (Richter 1958).

3.1 *Localisation of AE sources*

The first stage in the localisation method consists of recognising the data needed to identify the AE sources, followed by the triangulation procedure (Carpinteri et al. 2006). During the first stage, the groups of signals, recorded by the various sensors, that fall into time intervals compatible with the formation of microcracks in the volume analysed, are identified. These time intervals, of the order of microseconds, are defined on the basis of the presumed speed of transmission of the waves (P) and the mutual distance of the sensors applied to the surface of the material. It is common practice to consider the amplitude threshold of 100μV of the non-amplified signal to distinguish between P-wave and S-wave arrival times. In fact, P-waves are usually characterized by higher value signals. In the second stage, when the formation of microcracks in a three-dimensional space is analysed, the triangulation technique can be applied if the signals recorded by at least five sensors fall into compatible time intervals. Thus, with this procedure it is possible to define both the position of the microcracks in the volume and the speed of transmission of P-waves. The localisation procedure can also be performed through numerical techniques using optimisation methods such as the Least Squares Method (LSM) (Carpinteri et al. 2006).

3.2 *Moment tensor analysis*

Having identified the individual AE events through the localisation process, it is interesting to evaluate the orientation, the direction and the modes of the microcracks. Moment tensor analysis was developed in seismology to describe the mechanics of earthquakes (Aki & Richards 1980). The same method, transferred to the field of acoustic emissions, is able to represent a source of ultrasonic waves in terms of motion and orientation. From the theoretical standpoint, the procedure fine-tuned in this study relies from the theoretical standpoint on the procedure defined by Shigeishi and Ohtsu (2001). This procedure, called SiGMA, characterised the AE signal by taking into account only the first arrival time of P-waves. In this procedure the moment tensor components m_{pq} are proportional to the amplitudes $A(\mathbf{x})$ of the first P-waves to reach the transducers:

$$A(\mathbf{x}) = \frac{C_s \ REF(\mathbf{t},\mathbf{r})}{R}(r_1 \ r_2 \ r_3)\begin{pmatrix} m_{11} & m_{12} & m_{13} \\ m_{21} & m_{22} & m_{23} \\ m_{31} & m_{32} & m_{33} \end{pmatrix}\begin{pmatrix} r_1 \\ r_2 \\ r_3 \end{pmatrix}. \quad (1)$$

C_s in Eq. (4) is a calibration coefficient of the acoustic emission sensors, R is the distance between the AE source at point $\mathbf{y}$ and the sensor located at point $\mathbf{x}$. Vector $\mathbf{r}$ represents the components of the distances, R, obtained through the localisation procedure, and $REF(\mathbf{t},\mathbf{r})$ is the reflection coefficient of the sensitivity of the sensor between vector $\mathbf{r}$ and direction $\mathbf{t}$. The moment tensor provides a general representation of the seismic source. The seismic moment tensor is a variety of stress tensor for an elastic medium, similar to the stress tensor used in elastomechanics. Since the moment tensor is symmetrical, to be able to represent it, it is necessary to determine the six independent unknowns m_{pq}. To this end, in order to determine the components of the moment tensor, the amplitude of the signal $A(\mathbf{x})$ must be received from at least six AE channels. From an eigenvalue analysis of the moment tensor, it is possible to determine the type of crack localised:

$$\frac{\lambda_1}{\lambda_1} = X + Y + Z, \frac{\lambda_2}{\lambda_1} = 0 - \frac{Y}{2} + Z, \frac{\lambda_3}{\lambda_1} = -X - \frac{Y}{2} + Z, \quad (2)$$

where, λ_1, λ_2, λ_3 are the maximum, medium and minimum eigenvalues, respectively, X is the component due to shear, Y is the deviatoric tensile component, Z is the isotropic tensile component. Ohtsu classified an AE source with $X > 60\%$ as a shear crack, one with $X < 40\%$ and $Y + Z > 60\%$ as a tensile crack, and one with $40\% < X < 60\%$ as a mixed mode crack. Moreover, from an eigenvector analysis, it is possible to determine the versors, l and n, which determine the direction of the displacement and the orientation of the crack surfaces (Shigeishi & Ohtsu 2001).

4 AE DATA ANALYSIS

4.1 *Specimens PS6 and PN4*

Masonry test pieces PS6 and PN4 were monitored with the AE technique throughout the loading test. Figure 6 shows, for the PS6 specimen, the diagrams of the AE cumulative and differential counts vs. time obtained during the test. Since the imposed displacements and times are proportional, it is possible to compare the diagram in Figure 2 with that in Figure 6. It can be seen that cumulative counts increase, very slowly at first and then proportionally to the load, reaching a peak in the proximity of the highest load reached in the test. The function representing the differential counts (AE count number per minute), instead, reaches its maximum value in the ascending branch of the load-displacement curves and reduces quickly to nil in the proximity of the ultimate load. From the diagrams of the differential counts of the AE signals, it is therefore possible to identify two phases in the loading process: a first

phase during which the biggest cracks are formed and the material reaches a critical damage condition (phase 1), and a second phase during which the material tends to exhaust its bearing capacity (phase 2).

From the diagrams in Figure 6, it can also be seen that the material begins to release energy when the stress level, already reached in the uncracked specimen, is exceeded during the tests on the repaired specimen. In perfect agreement with the so-called *Kaiser effect* (Kaiser, 1950).
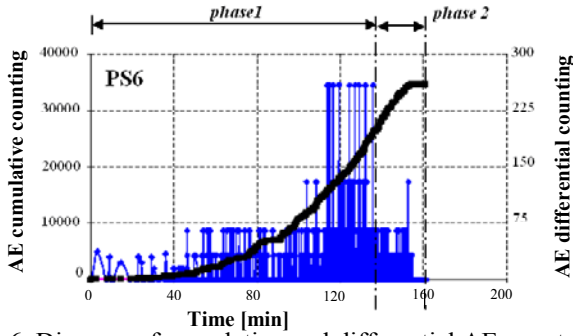

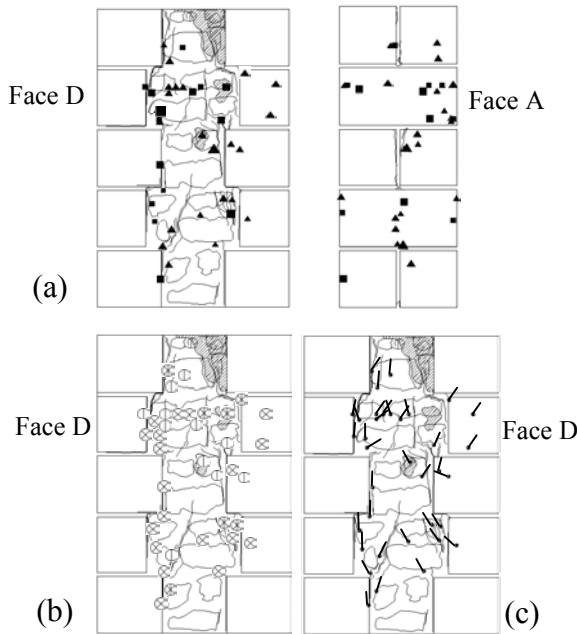Figure 6. Diagram of cumulative and differential AE counts for the PS6 specimen.

Figure 7. AE sources in specimen PS6. (a) Localization and magnitudes of relative crack volumes , (b) crack typology, (c) crack direction vectors.

Table 3. Markers of AE sources representing crack volume expansion in phase 1 and phase 2 of the test and labels identifying crack typology.

Phase 1		Phase 2	
▲	$\Delta V \leq 0.1$ mm³	■	$\Delta V \leq 0.1$ mm³
▲	$1 \leq \Delta V \leq 0.2$ mm³	■	$0.1 \leq \Delta V \leq 0.2$ mm³
▲	$\Delta V \geq 0.2$ mm³	■	$\Delta V \geq 0.2$ mm³
Crack Typology (Mode)			
shear ⊗	tensile ⬭		mixed ⊗

Figure 7 shows, on the A and D faces of specimens PS6, the projections of the AE sources identified during the loading test. In particular, during loading test 34, AE signal source points were identified (Fig. 7). The transmission speed of the ultra-

sonic signals was found to be ca 1350 m/s, the frequency ca 120 kHz. The sources determined during the first phase of the loading test (phase 1) are represented by triangles; the ones represented by squares were determined during phase 2, when the material tends to exhaust its bearing capacity (Table 3). During the load test on specimen PN4, instead, 32 source points were identified from AE signals. The transmission speed of the signals was found to be ca 980 m/s, the frequency was ca 90 kHz.

Damage process zones are in good agreement with the considerations expressed in Section 2.3. The higher speed of the signals in specimen PS6 compared to specimen PN4 should probably be ascribed to the greater compactness of Serena stone vs. Noto stone. AE signals, in fact, undergo a considerable attenuation in porous media.

4.2 *Estimating the volumes of the microcracks*

Shigeishi and Ohtsu (2001) pointed out that the trace component of the moment tensor can be expressed with the following relationship:

$$m_{kk} = (3\lambda + 2\mu)l_k n_k \Delta V, \qquad (3)$$

where λ and μ are Lamè's constants, l_k and n_k are the components of the direction vector and the vector normal to the surface of the crack, m_{kk} is the trace component of the moment tensor, and ΔV is the volume expansion of each microcrack. As a rule, in elasticity theory, factor $(3\lambda + 2\mu) = K$ is considered as a constant specific to each material. Volume expansion may therefore be expressed as follows:

$$\Delta V = \frac{1}{K} \frac{m_{kk}}{l_k n_k}. \qquad (7)$$

For specimen PS6 in Serena stone, considering an average elastic modulus $E \cong 2000$ N/mm² and a Poisson coefficient of 0.2 (Table 1), we get $\lambda = E\nu/(1+\nu)(1-2\nu) \cong 5700$N/mm² and $\mu = E\nu/2(1-2\nu) \cong 1700$N/mm², which means it is possible to assume an approximate value of $K_S \cong 20000$ N/mm². Similarly, for specimen PN4 in Noto stone, the value of $K_N \cong 3800$ N/mm² can be determined.

Assuming term K to be approximately constant for both specimens throughout the loading tests, it can be seen that the highest magnitude volume expansion events are concentrated at the macrocracks identified. If the AE sources are identified by means of a graphic representation where individual crack magnitudes are symbolised, an interesting superposition is obtained between the AE sources with large crack volumes and the failure planes visible to the naked eye (Fig. 7). For specimen PS6, crack volume magnitudes, broken down by loading phase, are represented according to the notation listed in Table 3. Figure 7 also illustrates crack types and the crack direction vectors.

5 STATISTICAL DISTRIBUTION OF AE EVENTS

By analogy with seismic phenomena, in the AE field, magnitude is defined as follows:

$$m = Log_{10}A_{max} + f(r),\qquad(4)$$

where, A_{max} is the amplitude of the signal expressed in μV, and $f(r)$ is a correction coefficient whereby signal amplitude is taken to be a decreasing function of the distance r between the source and the AE sensor. The empirical Gutenberg-Richter law (Richter 1950) give:

$$Log_{10}N(\geq m) = a - bm \text{ or } N(\geq m) = 10^{a-bm},\qquad(5)$$

where N is the cumulative number of earthquakes with magnitude $\geq m$ in a given area and a specific time-range, whilst b and a are positive constants varying from one region to another. Eq. (5) has been used successfully in the AE field to study the scaling laws of AE wave amplitude distribution. According to Eq. (5), the "b-value" stands for the slope of the regression line in the "log-linear" diagram of AE signal amplitude distribution. This parameter changes systematically at different times in the course of the damage process and therefore can be used to estimate damage evolution modalities.

Moreover, scale effects on the size of the cracks identified with the AE technique entail, by analogy with earthquakes (Carpinteri et al. 2006), the validity of the following relationship:

$$N(\geq L) = cL^{-2b},\qquad(6)$$

where N is the cumulative number of AE generated by cracks having a characteristic size $\geq L$, c is the total number of AE events and $D = 2b$ is the noninteger exponent of the distribution. The cumulative distribution (6) is substantially identical to the one proposed by Carpinteri (1994), according to which the number of cracks with size $\geq L$ contained in a body is given by:

$$N^*(\geq L) = N_{tot} L^{-\gamma}.\qquad(7)$$

In Eq. (7), γ is an exponent reflecting the disorder, i.e., crack size scatter, and N_{tot} is the total number of cracks contained in the material. By equating distributions (6) and (7), we find that: $2b = \gamma$. At collapse, when the size of the largest crack is proportional to the characteristic dimensions of a structure, function (7) is characterised by an exponent $\gamma = 2$, corresponding to $b = 1$. In (Carpinteri 1994) it is also demonstrated that $\gamma = 2$ is a lower limit corresponding to the minimum value $b = 1$, observed experimentally when the bearing capacity of a structural member is exhausted.

By applying these concepts to the analysis of the "b-value" of specimens PS6 and PN4, it can be seen that the former exhausted its bearing capacity during the load test, with the formation of cracks of a size comparable to that of the specimen, along the interface between the filler and the outer wall (b-value $\cong$ 1), and the latter, characterised by a widespread cracking pattern, still has a reserve of strength before reaching the final collapse (b-value $\cong$ 1.7). The determination of the "b-values" for the two specimens is shown in Figure 8.
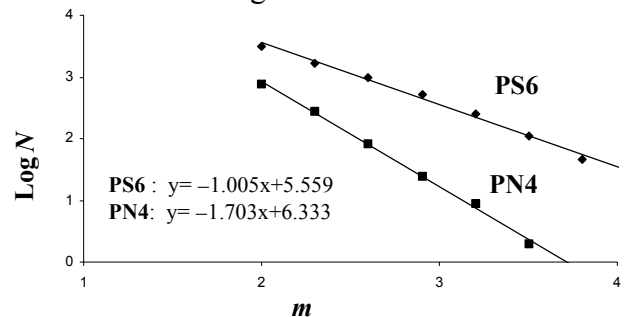

PS6 : y= −1.005x+5.559
PN4 : y= −1.703x+6.333

Figure 8. Determination of the "b-value" at the end of the loading test on the two specimens.

6 ACOUSTIC EMISSION AS SELF ORGANIZED CRITICALITY.

In works by authors such as Chen and Bak (Chen et al.1991) it is pointed out that the occurrence of seismic events on a geophysical scale, or the cracking of rock specimens subjected to stress conditions in laboratory tests, may be interpreted as instances of Self Organized Criticality (SOC) phenomena. The concept of SOC implies that, in a system evolving in permanently critical conditions, the disturbances localised in a portion of the system may have cascade effects on the entire system. In this context, SOC state anomalies play the role of precursors of catastrophic behaviour. SOC behaviour is a permanent competition between the action of the process driving forces and the response of the system's dynamics. The determination of the time series power law exponent, referred to as Hurst exponent, can facilitate the identification of the self-organised nature of these phenomena (Hurst et al. 1965).

6.1 Hurst exponent of AE time series

The AE signal time series obtained from specimens PS6 and PN4 were interpreted by analysing the Hurst exponent. The starting consideration is that evolutive phenomena accompanied by a long-term memory of earlier states − such as a loading process culminating in the failure of a structural element − departs from a Gaussian random sequence type behaviour. In physics, this sequence is identified, for example, by the Brownian motion of a particle submerged in a fluid (Einstein 1916). Moving in an erratic fashion, this particle covers a distance, which, on average, is a function of the square root of time multiplied by a constant:

$$R = k\,t^{1/2}. \qquad (8)$$

In Eq. (8), R is the distance covered, t is the time and k is a constant. In a generalised form, Eq. (8) can be rewritten as follows:

$$R/S \propto \tau^{H}, \qquad (9)$$

where τ is the time associated with a certain time window and H is the Hurst exponent. $R(N)$ and $S(N)$ are defined as:

$$R(N) = \max_{1 \le j \le N}\left\{\sum_{i=1}^{j}(A_i - \overline{A})\right\} - \min_{1 \le j \le N}\left\{\sum_{i=1}^{j}(A_i - \overline{A})\right\}, \qquad (10)$$

$$S(N) = \sqrt{\sum_{i=1}^{N}(A_i - \overline{A})^2}. \qquad (11)$$

In Eqs. (10) and (11), $R(N)$ and $S(N)$ stand for the range and the standard deviation of the historical time series in question, while N and $\overline{A}$ are, respectively, the length and the mean value of the sequence A_i in a time window τ. The range, $R(N)$, is obtained as the difference between the maximum and the minimum value of the cumulated summation of the deviations from the mean of all sample observations. Hence, by determining the ratio between $R(N)$ and $S(N)$ it becomes possible to standardise the measurements and compare the results of different analyses (Rescaled Range Analysis).

In general, R/S increases with increasing τ, according to a power law, which is a function of H, and this exponent reflects the greater or lesser persistence of the phenomenon considered (Mandelbrot 1997). Moreover, H lies between the values 0 and 1; $H > 1/2$ corresponds to a persistent variation of the function: the greater is τ, the more probable is its further increase: $H \le 1/2$ characterizes an "anti-persistent" behaviour: the greater is τ, the more probable is a decrease in the function; $H = 1/2$ represents the Gaussian random sequence.
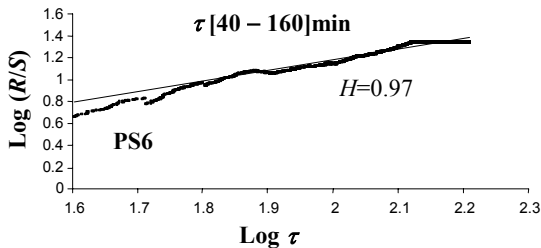
Figure 9. R/S analysis data sets for specimen PS6. The straight line shows the power law $R/S \propto \tau^{H}$, Eq. (9).

By analysing the AE data time series obtained from specimen PS6, for a time window of between 40 and 160 min (Fig. 9), i.e., extending from a few minutes of the start of the test till the end of the test, the Hurst exponent was found to be 0.97. This value remains virtually constant even for time windows of

decreasing size, starting from the initial instant of the analysis. Similar results were also obtained for specimen PN4.

It may be inferred that imposed deformation tests carried out through the application of a constantly increasing load display a persistent behaviour on the different time scales. This conclusion is highly relevant to the interpretation of structural damage phenomena and the monitoring of structures, possibly on site, with the AE technique, where the persistence of the energy released during the damage process may be used for predictive purposes when dealing with self-organised phenomena leading to collapse.

6.2 Hurst exponent of rupture profiles

Recently developed theoretical models have acquired increasing relevance in the study of seismicity. Some authors (see Hallgass et al. 1996) assumed that fault profiles can be regarded as fractals, and, in particular, as statistically self-affine profiles $F_H(t)$, whose roughness depends on the time scale as $|F_H(t+\tau) - F_H(t)| \sim \tau^{H}$. The exponent $0 \le H < 1$, in this case, controls the roughness of the fault where the standard Brownian profile corresponds to $H = 1/2$, and a differentiable limit curve corresponds to $H = 1$. More generally, the fractal dimension of the profile is well known to be $D_F = d - H$, in which the fractal ensemble is embedded in a d-dimensional Euclidean space. For a self-affine rough surface, the Euclidean reference dimension is $d = 3$. If one considers instead a representative profile of this surface we get $d = 2$. In either case, exponent H does not depend on the reference dimension (Zavarise et al. 2006).
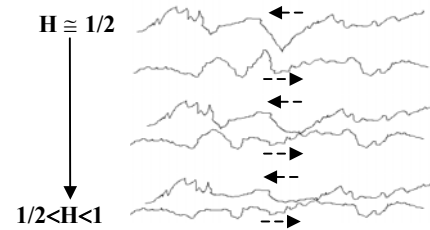

Figure 10. Process of mutual sliding between two facing faults. The Hurst exponent approaches 1 with decreasing profile roughness.

The laboratory tests performed on multi-leaf specimens PS6 and PN4 entailed, due to the testing modalities, a phenomenon of mutual sliding between outer and inner leaves (Fig. 1). Hence, the failure mechanism involved is similar to that of facing faults as shown in Figure 10. In either mechanism, failure is accompanied by a decrease in the roughness of the profiles in contact. Based on the foregoing, the variation in the Hurst exponent can be seen as a significant indicator of the failure process.

The b-value of the GR law and the Hurst exponent can be correlated during the damage process. The article by Hallgass et al. 1996 gives the following relationship:

$$\frac{b}{c} = 1 - \frac{H}{d-1}. \qquad (12)$$

In Eq. (12), c is the slope in the linear-log graph of the Richter law that correlates the magnitude of earthquakes with seismic energy (Richter 1958):

$$Log_{10}E = q + cm. \qquad (13)$$

Eq. (13) applied to the AE technique correlates the energy released by AE with magnitude m calculated as in Eq. (4). Accordingly, b-value and parameter c were computed by subdividing the test into homogenous time intervals. By introducing these values into Eq. (12) together with the Euclidean dimension, $d = 3$, we get the H vs. b-value diagram shown in Figure 11.

From Figure 11 it can be seen that for both specimens, when the b-value approaches 1, i.e., in the proximity of critical conditions, the roughness exponent H approaches 1. The physical meaning of this relationship lies in the fact that the surfaces in contact of the specimen leaves become smoother and smoother, causing a critical sliding rate up to collapse. The values of H computed at the start of the tests, when the b-values are high, provide an indication of the initial roughness of the faults as well as of the volumetric energy dissipation. At the end of the tests, the maximum value of H reached in PS6 turned out to be greater than that reached in PN4. This result regarding the roughness of the surfaces in contact corroborates the observations made in Section 5.
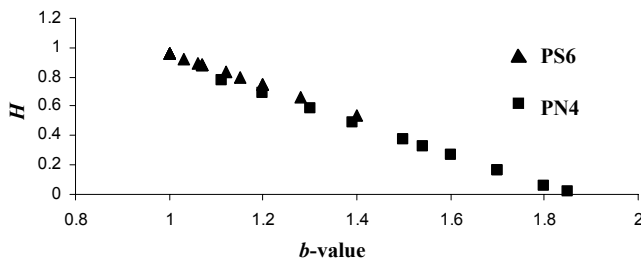

Figure 11. Exponent H vs. b-value from the tests performed on specimens PS6 and PN4.

7. CONCLUSIONS

An experimental research was carried out on repaired three-leaf walls reproducing the masonry types commonly used in Italian historical centres. The damage process zones, identified in the specimens through the AE technique, were in good agreement with the results of the tests performed by means of displacement transducers. The statistical techniques derived from seismology, such as the Gutenberg-Richter (GR) law, and the analysis performed in term of Self Organized Criticality (SOC), mated to AE monitoring, made it possible to interpret the damage mechanisms and to evaluate the efficiency of repair interventions, contributing to the identification of the most effective methodology for their optimisation.

REFERENCES

Aki, K. & Richards, P. G. 1980. *Quantitative Seismology, Theory and Method*. New York: W. H. Freeman.

Anzani, A. Binda, L. Fontana, A. Pina-Henriques, J. 2004. An experimental investigation on multiple-leaf stone masonry. *13th Int. Brick/Block Masonry Conference RAI Amsterdam, 4-7 July 2004.*

Binda, L. Anzani, A. Fontana, A. 2003. Mechanical behaviour of multiple-leaf stone masonry: experimental research. *3-Day Int. Conf. Structural Faults & Repair, London, 1-3 July 2003*, MC Forde (Ed.), Engineering Technics Press, Edinburgh, ISBN 0-947644-53-9, CD-ROM, Keynote Lecture.

Carpinteri, A. 1994. Scaling laws and renormalization groups for strength and toughness of disordered materials. *International Journal of Solids and Structures* 31: 291-302.

Carpinteri, A. & Lacidogna, G. 2006. Damage monitoring of an historical masonry building by the acoustic emission technique. *Materials and Structures* 20: 143-149.

Carpinteri, A. Lacidogna, G. Niccolini, G. 2006. Critical behaviour in concrete structures and damage localization by acoustic emission. *Key Enineering Materials* 312: 305-310.

Carpinteri, A. Lacidogna, G. Pugno, N. 2007. Structural damage diagnosis and life-time assessment by acoustic emission monitoring. *Engineering Fracture Mechanics* 74: 273-289.

Chen, K. Bak, P. Obukhov, S. 1991. Self-organized criticality of the fracture process in rock. *Phys Rev A* 43 625.

Einstein, A. 1916. *Investigations on the Theory of Brownian Movement*. NewYork: Dover, essay I and II.

Hallgass, R. Loreto, V. Mazzella, O. Paladin, G. and Pietronero, L. 1996. Earthquakes statistics and fractal faults. *Physical Review E* 56:1346-1256.

Hurst, H.E. Black, R.P. Simaika, Y.M. 1965. *Long Term Storage. An Experimental study*. London: Constable.

Kaiser, J. 1950. *An investigation into the occurrence of noises in tensile tests, or a study of acoustic phenomena in tensile tests*. Ph.D, Technische Hochschule München: Munich FRG.

Mandelbrot, B. 1997. *Fractals and Scaling in Finance*, New Yor: Springer-Verlag.

Modena, C. Valluzzi, M.R. Tongini Folli, R. Binda, L. 2002 Design Choices and Intervention Techniques for Repairing and Strengthening of the Monza Cathedral Bell-Tower, *Construction Building Materials*, ISSN 0950-0618, Special Issue, 16(7):385-395.

Richter, C. F. *1958 Elementary Seismology*. S. Francisco and London: W.H. Freeman and Company.

Shigeishi, M. & Ohtsu, M. 2001. Acoustic emission moment tensor analysis: development for crack identification in concrete materials. *Construction and Buildings Materials* 15: 311-319.

Zavarise, G. Borri-Brunetto, M. Paggi, M. 2007. On the resolution dependence of micromechanical contact models. *Wear* 262:42-54.